ABSTRACT

Paleogene Climate Reconstruction Using Paleosol Mineral Assemblages,
San Juan Basin, New Mexico

Nicole A. Price, M.S.

Mentor: Steve Dworkin, Ph.D.

Certain preserved minerals are stable within specific climate conditions, thus their presence can indicate the type of climate that was present during their deposition. The climate after the Cretaceous/Paleogene extinction event is unique based upon preceding circumstances and thus requires analysis. Through the analysis of outcrops within the Nacimiento Formation of the San Juan Basin, New Mexico, the paleoclimate of this time period can be reconstructed. This is done through X-ray diffractometry, where climatically significant minerals can be identified and quantified to lead to a conclusion. It had been discovered that kaolinite, one such mineral climate indicator, was present throughout all of the observed sections, indicating the climate was never completely dry. However, some sections contained more kaolinite than others, indicating varied climate across regions, but note that the climate was never dry due to the lack of calcite present. Thus, the climate was wet during the Nacimiento deposition.

Paleogene Climate Reconstruction Using Paleosol Mineral Assemblages, San Juan Basin, New Mexico

by

Nicole Ashley Price, B.S.

A Thesis

Approved by the Department of Geosciences

Joe Yelderman, Ph.D., Chairperson

Submitted to the Graduate Faculty of
Baylor University in Partial Fulfillment of the
Requirements for the Degree
of

Master of Science

Approved by the Thesis Committee

Steve Dworkin, Ph.D., Chairperson

Dan Peppe, Ph.D.

Kevin Kladsmeyer, Ph.D.

Accepted by the Graduate School
May 2022

J. Larry Lyon, Ph.D., Dean

Page bearing signatures is kept on file in the Graduate School.

TABLE OF CONTENTS

LIST OF FIGURES

LIST OF TABLES

ACKNOWLEDGMENTS

The author would like to convey her overwhelming gratitude to Dr. Steve Dworkin and Dr. Dan Peppe, for their support and guidance, and without whom this project would have never been possible.

DEDICATION

To Jim and Christina for supporting my endeavors in life and guiding me to this moment.

I would also like to dedicate this paper to Katie for always supporting me and for being the role model I needed in life. You have inspired me to reach ad astra per aspera.

CHAPTER ONE

Introduction

This study investigates early Paleogene climate using paleosol mineral assemblages from the Nacimiento Formation in the San Juan Basin, New Mexico. Additionally, the role that landscape position plays in soil-weathering intensity will be explored by comparing paleosol mineral assemblages across four time-correlative sites of the Nacimiento Formation: Kimbeto Wash, Betonnie Tsosie, Mesa De Cuba, and the De-Na-Zin (Figure 2.1). The paleosols studied at these sites span approximately the same interval of time from ~65.8 - 64.4 Ma (Flynn et al., 2020; Cather et al., 2019). This study is important because the San Juan Basin provides a record of climatic conditions in North America shortly after the Cretaceous/Paleogene (K/Pg) extinction event.

This project uses a novel method of assessing mineral assemblages in paleosols to reconstruct paleoclimatic conditions. Soil mineral assemblages, which are a function of the climate in which they formed (Chadwick & Chorover, 2001), can be used to reconstruct Earth's climate if they are preserved in the rock record as a paleosol mineral assemblage (PMA). PMA's provide evidence of the climate-driven weathering reactions that destroy soil parent material and the equally climate-sensitive creation of solid weathering products (pedogenic minerals). The soil-mineral pedogenic thresholds identified by the PMA represent climate-controlled limits for chemical-weathering reactions resulting in distinct mineral assemblages that can be used to interpret evolving environmental conditions.

This study summarizes the geologic setting of the San Juan Basin and then investigates the mineralogy and age of a series of paleosols that span a small time interval of the early Paleogene. The mineralogy of the paleosols are characterized using quantitative X-ray diffraction and then compare to each other using an age model developed using magneto stratigraphy. The results of this analysis depict how the mineral abundances in each of the paleosols reflects evolving environmental conditions in the San Juan Basin. This study shows how increasing Mean Annual Precipitation (MAP) over a short time interval influenced the weathering intensity within the San Juan Basin shortly after the K/Pg boundary.

CHAPTER TWO

Geologic Background and Setting

The San Juan Basin is located primarily in northwestern New Mexico, and partially in southwestern Colorado (Figure 2.1). The basin extends over 19,425 square kilometers and is about 161 kilometers from north to south, and about 145 kilometers from east to west (Fassett et al., 1971). This foreland basin formed as a result of deformation associated with the Laramide Orogeny and contains rocks that range in age from the Cambrian through the Neogene (Cather et al., 2004). Within the study area, outcrops of the Nacimiento and Ojo Alamo Formations represent deposition that is nearly continuous over a several million-year history in the early Paleocene (Flynn et al., 2020) (Figure 2.1).

The Nacimiento Formation is lower Paleocene in age and represents an important time period because it comprises the environmental conditions that existed after the major extinction event at the K/Pg boundary. Broadly, the climate of the early Paleocene was warm, moderately wet and seasonally dry (Davis et. al 2016; Flynn and Peppe, 2019). Faunal, floral, and paleosol evidence suggests that the climate of the San Juan Basin in the early Paleogene was relatively stable (Davis et. al 2016, Flynn and Peppe, 2019) and this research project will investigate if any climate variations can be detected.

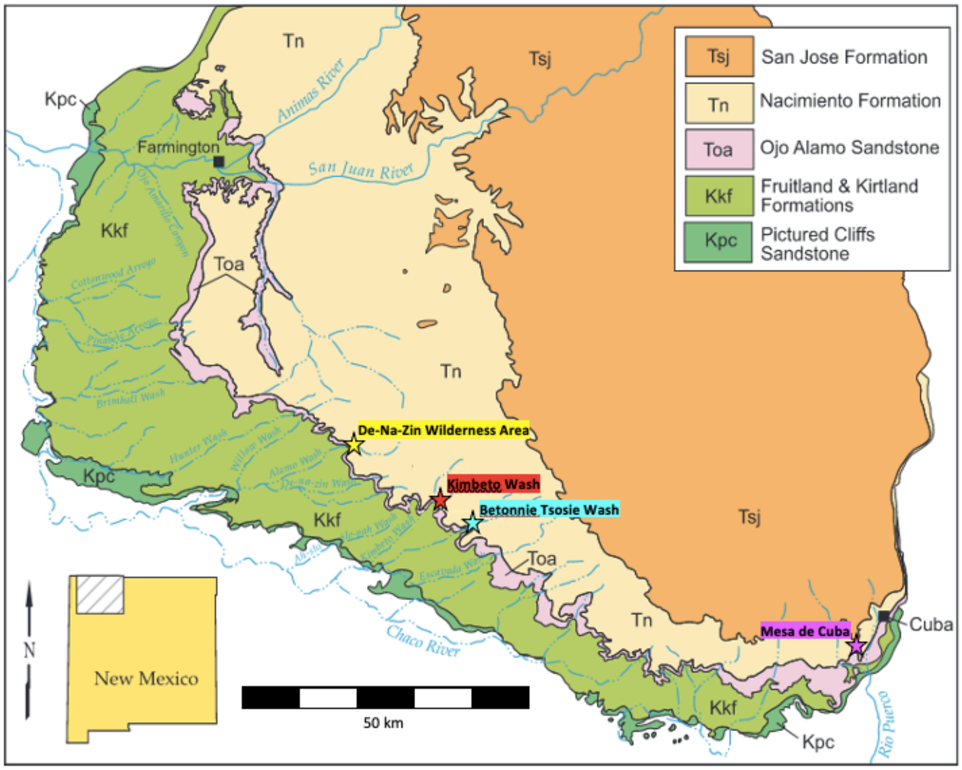

Figure 2.1. A geologic map of the San Juan basin and its strata from the Upper Cretaceous through the lower Eocene. The red star on the map show the location of the Kimbeto Wash site, the pink star represents the Mesa De Cuba site, the yellow star shows the De-Na-Zin site, and the teal star indicates the Betonnie Tsosie outcrop (modified from Willamson et al., 2008).

CHAPTER THREE

Methods

The samples used in this study were collected by Adam Davis as part of his analysis of depositional environments and paleopedology of the Nacimiento and Ojo Alamo Formations (Davis et al., 2019). These rocks have been put into a magnetostratigraphic framework (Flynn et al., 2020) which provides age control for the paleoclimate reconstruction.

Paleosols collected from the various lithofacies present in the Nacimiento Formation are mostly composed of vertisols and inceptisols, except for one entisol identified within the Kimbeto Formation for sample P1.1. Different lithofacies and good stratigraphic coverage were needed when choosing paleosols to be sampled; specifically paleosols with a vertisol soil type and palesols containing silcrete. Restricting sampled paleosols to mostly verstisols helped to ensure that paleosol maturity was similar between samples.

The paleosol mineral assemblage for each paleosol has been determined using quantitative X-ray diffraction (XRD) techniques. The laboratory technique is time consuming and includes the following steps. The samples are first prepared by drying and crushing in a mortar and pestle. The crushed paleosol material is then passed through a 0.4mm sieve onto weighing paper and 3.00g of this material is transferred into a micronizing jar along with 0.75g of Al_2O_3. 5 ml of methanol is added to the micronizing jar, which is then milled for a total of 5 minutes. The crushed mixture is then dried in a fume hood for 24 hours to allow the methanol to evaporate. Once the sample is dry it is gently disaggregated using a mortar and pestle and then passed through a 250 micron sieve and then placed into a small plastic vial with a beater bead in it. One ml of vertrel is added to the vial which is then placed into the bead beater machine for 10 minutes. The fully pulverized fine powder is transferred into a labeled glass vial for subsequent XRD analysis. A randomly oriented powder mount is made with the crushed sample which is then X-rayed from 5 to 65 degrees two-theta with a step size of 0.02 degrees two-theta and a count time of two seconds per step. The resulting digital diffraction pattern is then uploaded into the Rock Jock program (Ebrel, 2003) which identifies and quantifies the abundance of the minerals that are present using whole pattern matching techniques coupled with the reference intensity ratio method.

The age of individual samples was calculated used sediment accumulation rates that were determined through local magnetostratigraphy (Flynn et al., 2020). Sediment accumulation rates from Flynn et al. (2020) were updated using chron durations and ages from the 2020 Geomagnetic Polarity Time Scale (Ogg J. G., 2020). All samples in this study were from sections correlated to polarity sub-chrons C29r, C29n, C28r, and C28n (Figures 3.3-3.6; Flynn et al., 2020).

Specifically, the stratigraphic distance between the sample and local chron boundaries was used to determine the age of each paleosol sample. To determine the age of each sample, the equation below was used.

$$\frac{\text{(Stratigraphic position of sample - Stratigraphic position of chron boundary)}}{Sediment\ accumulation\ rate} = age\ of\ paleosol$$

Based on sediment accumulation rates, the age of paleosol samples ranges from 65.33-64.74 Ma for the Kimbeto section, 65.07-64.64 Ma for the Mesa De Cuba, 65.84-64.86 Ma for Betonnie Tsosie, and 65.85-65.36 Ma for the De-Na-Zin (Figures 3.1 and 3.2).

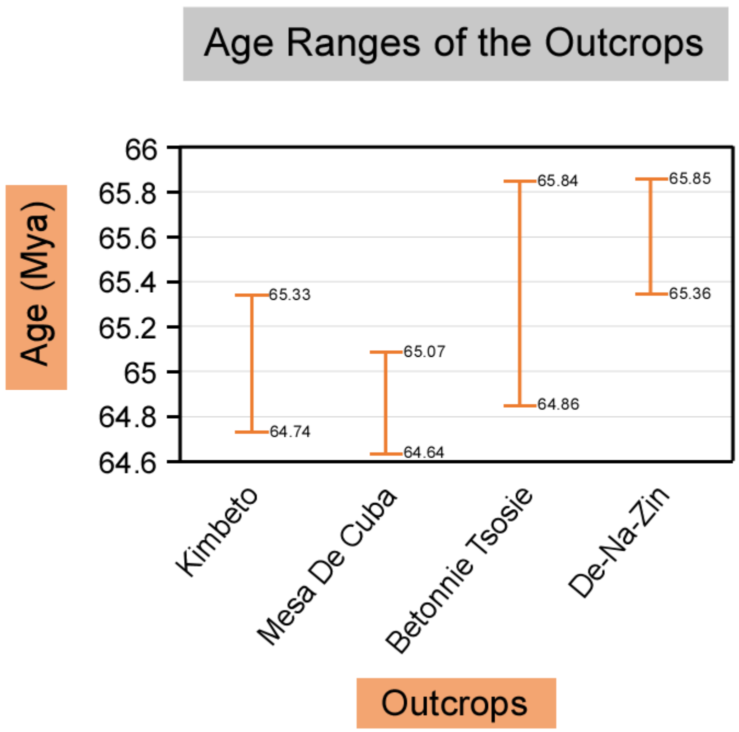

Figure 3.1. A chart depicting the age ranges for each outcrop and where they overlap. Age units depicted are millions of years ago (Ma).

Paleosol Age Estimates							
Kimbeto		Mesa De Cuba		Betonnie Tsosie		De-Na-Zin	
Sample ID	Age(Mya)	Sample ID	Age(Mya)	Sample ID	Age(Mya)	Sample ID	Age(Mya)
P1.1	65.33	P3.3	65.08	P1	65.84	A	65.85
P6.1	65.24	P4.3	64.92	P4	65.74	C	65.75
P8.1	65.16	P6.3	64.85	P9	65.57	D	65.68
P9.1	64.99	P9.3	64.82	P12	65.52	E	65.54
P10.1	64.98	P11.3	64.75	P14	65.34	F	65.45
P15.1	64.87	P15.3	64.70	P17	65.18	C11	65.36
P19.1	64.85	P17.3	64.69	P19	65.16	-	-
P21.1	64.83	P20.3	64.66	P21	65.09	-	-
P22.1	64.82	P21.3	64.65	P24	65.04	-	-
P23.1	64.80	-	-	P27	64.98	-	-
P24.1	64.79	-	-	P29	64.86	-	-
P27.1	64.76	-	-	-	-	-	-
P28.1	64.75	-	-	-	-	-	-
P29.1	64.74	-	-	-	-	-	-

Figure 3.2. Paleosol age estimates for each outcrop observed.

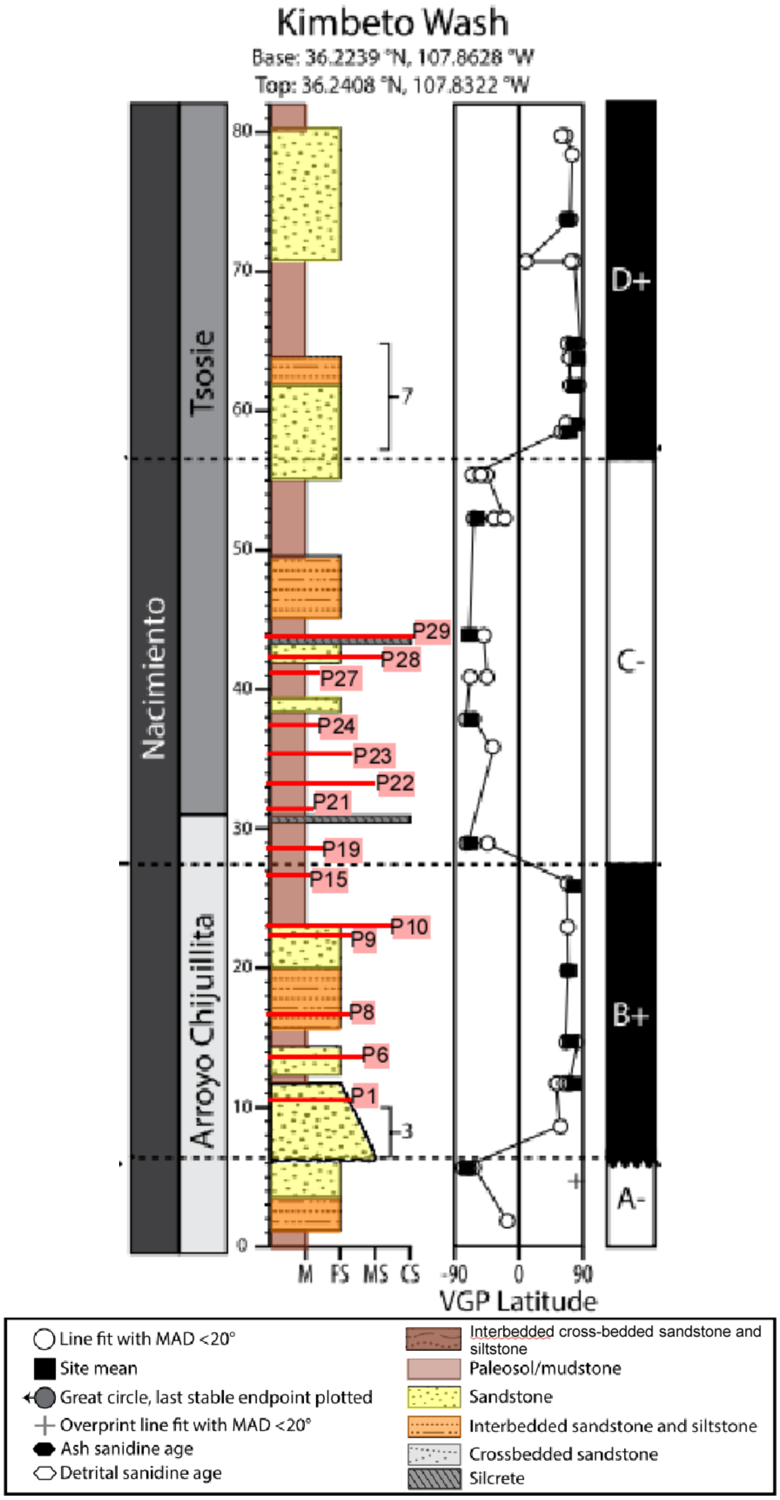

Figure 3.3. A measured section from Kimbeto Wash showing the location of 14 samples analyzed for this study relative to the local polarity stratigraphy (modified from Flynn et al., 2020).

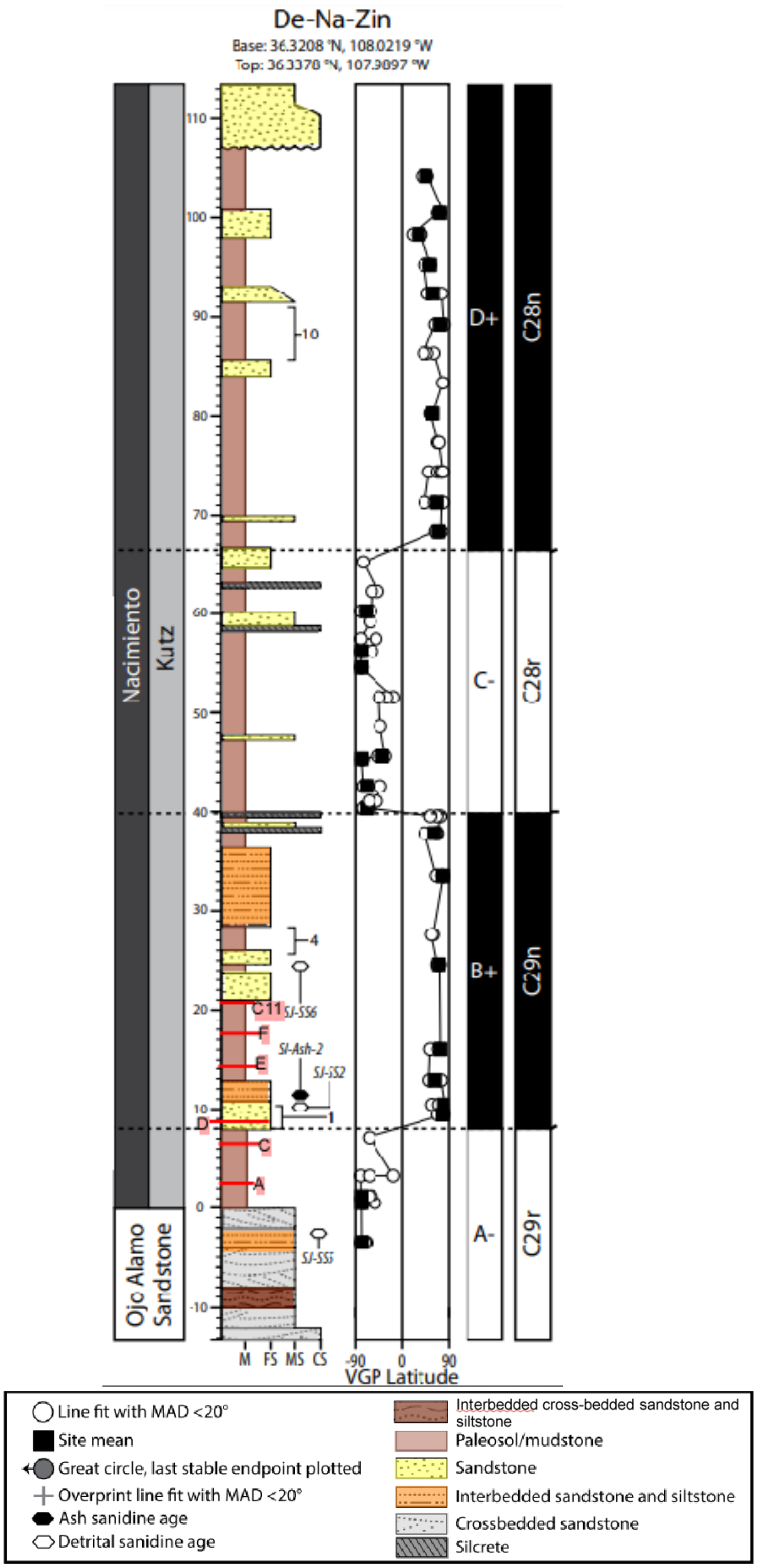

Figure 3.4. The measured section from the De-Na-Zin showing the location of 6 samples analyzed for this study (modified from Flynn et al., 2020).

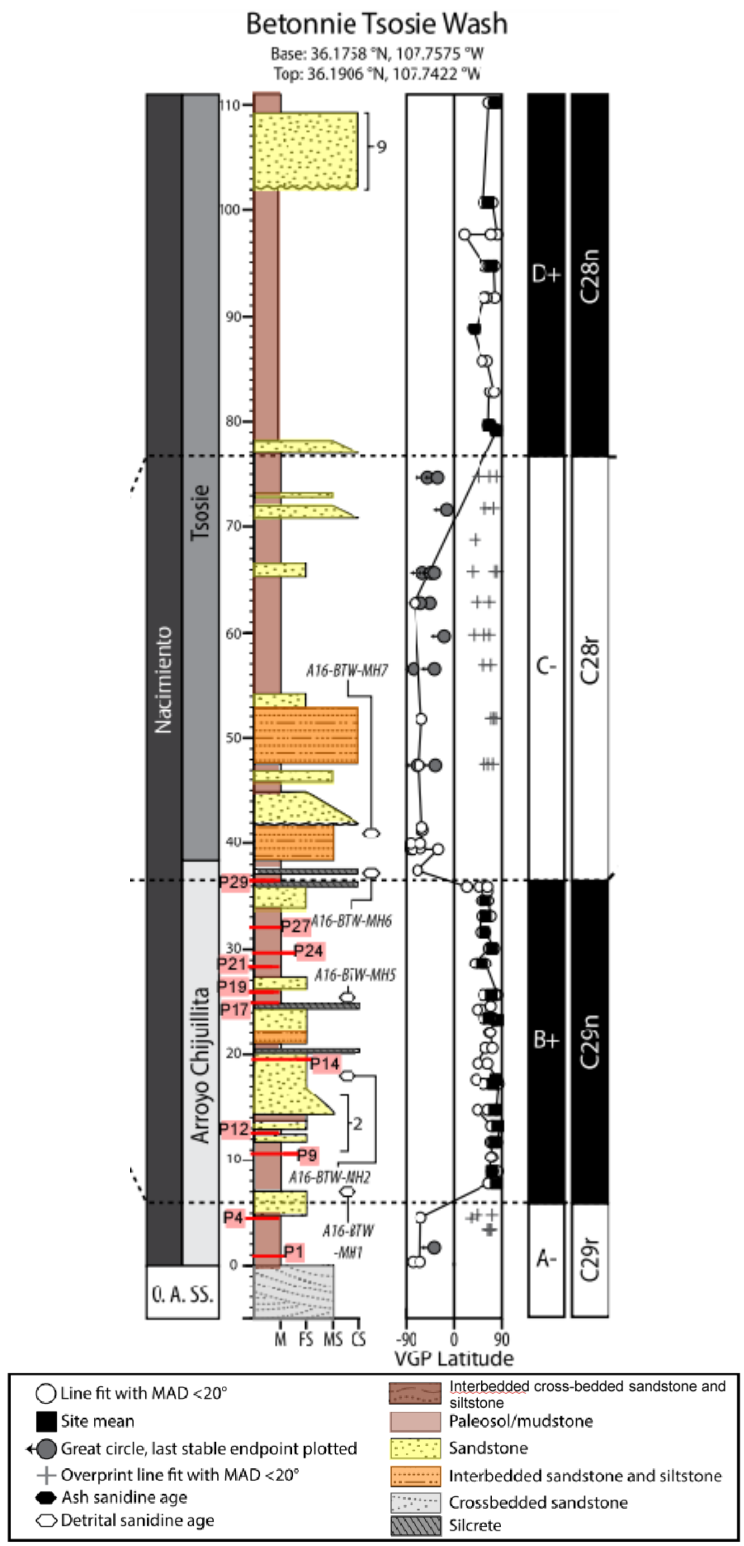

Figure 3.5. The measured section from the Betonnie Tsosie showing the location of 11 samples analyzed for this study relative to the local polarity stratigraphy (modified from Flynn et al., 2020).

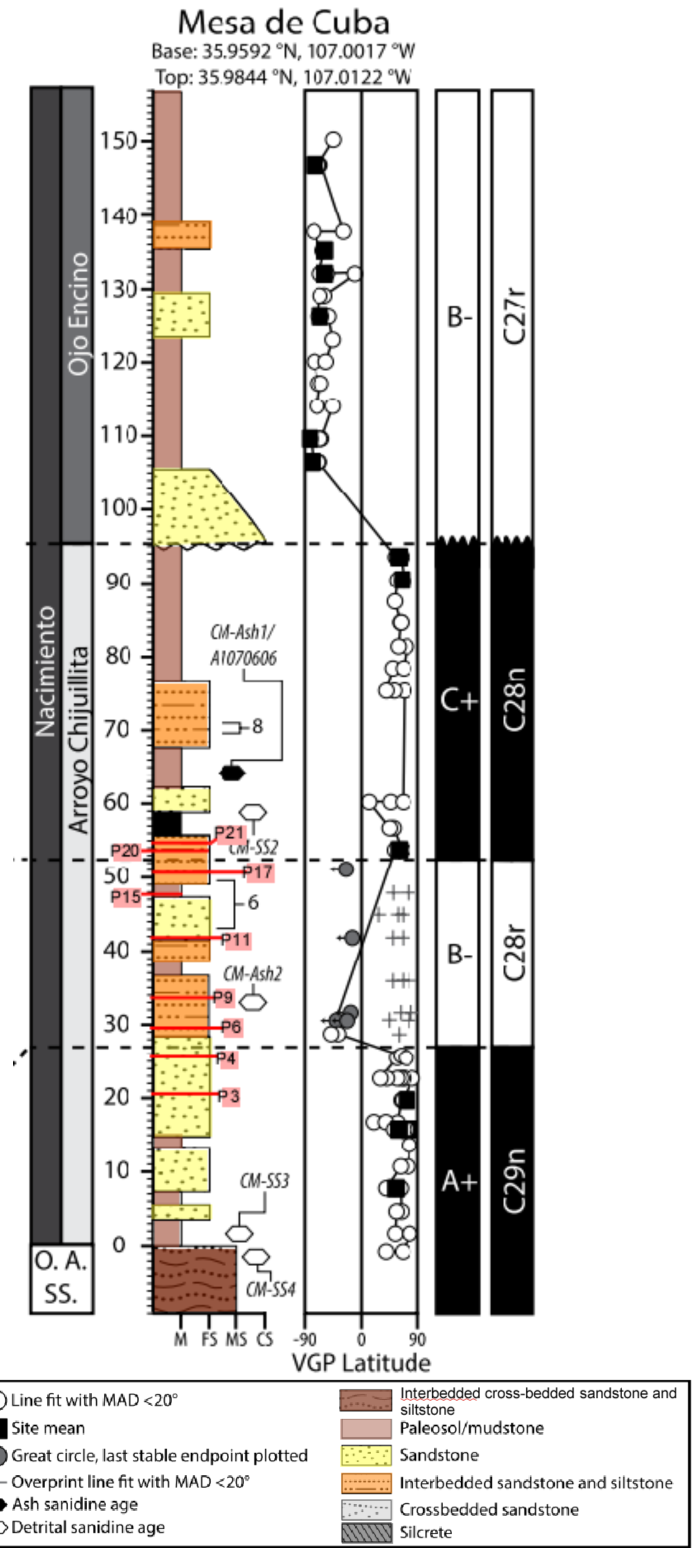

Figure 3.6. The measured section from the Mesa De Cuba showing the location of 9 samples analyzed for this study relative to the local polarity stratigraphy (modified from Flynn et al., 2020).

CHAPTER FOUR

Results

The minerals identified using X-ray diffraction include Fe oxy/hydroxides, kaolinite, smectite, illite, sanidine, other potassium feldspars, plagioclase, quartz, and muscovite. The most abundant mineral in the paleosols is smectite and it varies between 17.6 and 64.8 Wt% with an average value of 38.8 Wt% (Figure 4.1). Other abundant paleosol minerals include quartz (11.3 to 49.4 Wt%, average of 21.9 Wt%), plagioclase (0 to 29.4 Wt%, average 7.1 Wt%), illite (0 to 25.3 Wt%, average 11.8 Wt%), and kaolinite (0 to 15.8 Wt%, average 5.5 Wt%). Muscovite makes up an average of 5.6 Wt% of the paleosols and hematite is the least abundant pedogenic mineral and is usually present in abundances less than 1wt % and has an average of 0.6 Wt%.

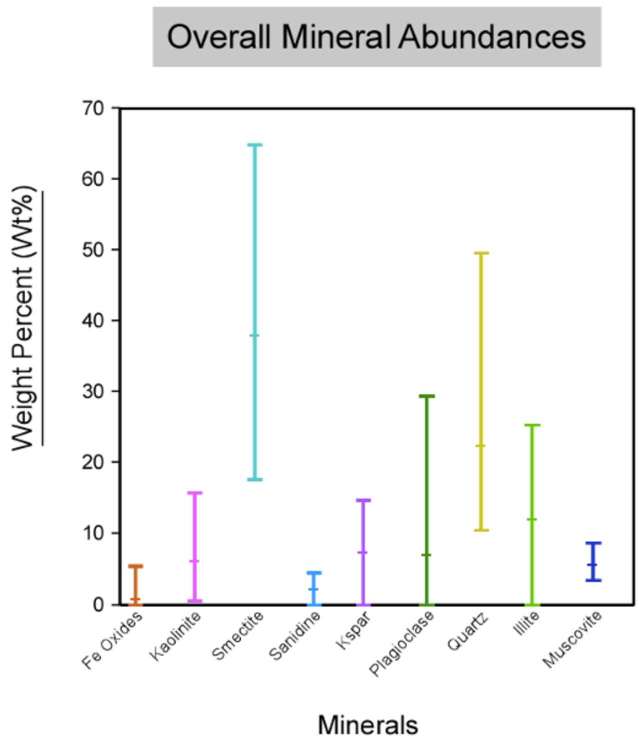

Figure 4.1. Range of abundances of minerals in Naciemento paleosols with the average indicated by a line in the middle of the mineral range.

Figures 4.2, 4.3, and 4.4 show these data stratigraphically and Tables 4.1, 4.2, 4.3, and 4.4 present the raw data.

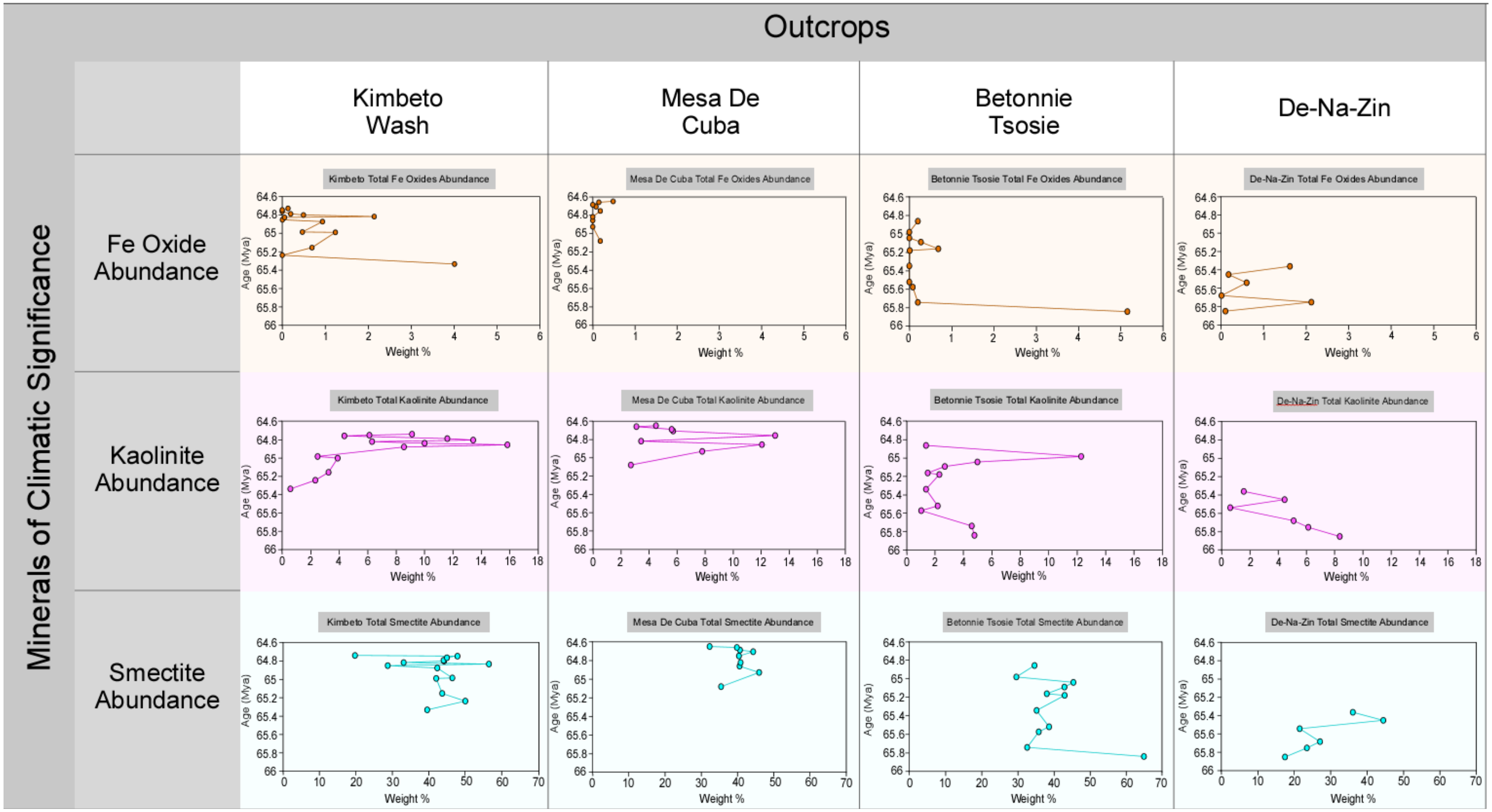

Figure 4.2. Stratigraphic occurrence of pedogenic minerals that are sensitive to climate conditions and are likely to be neoformed

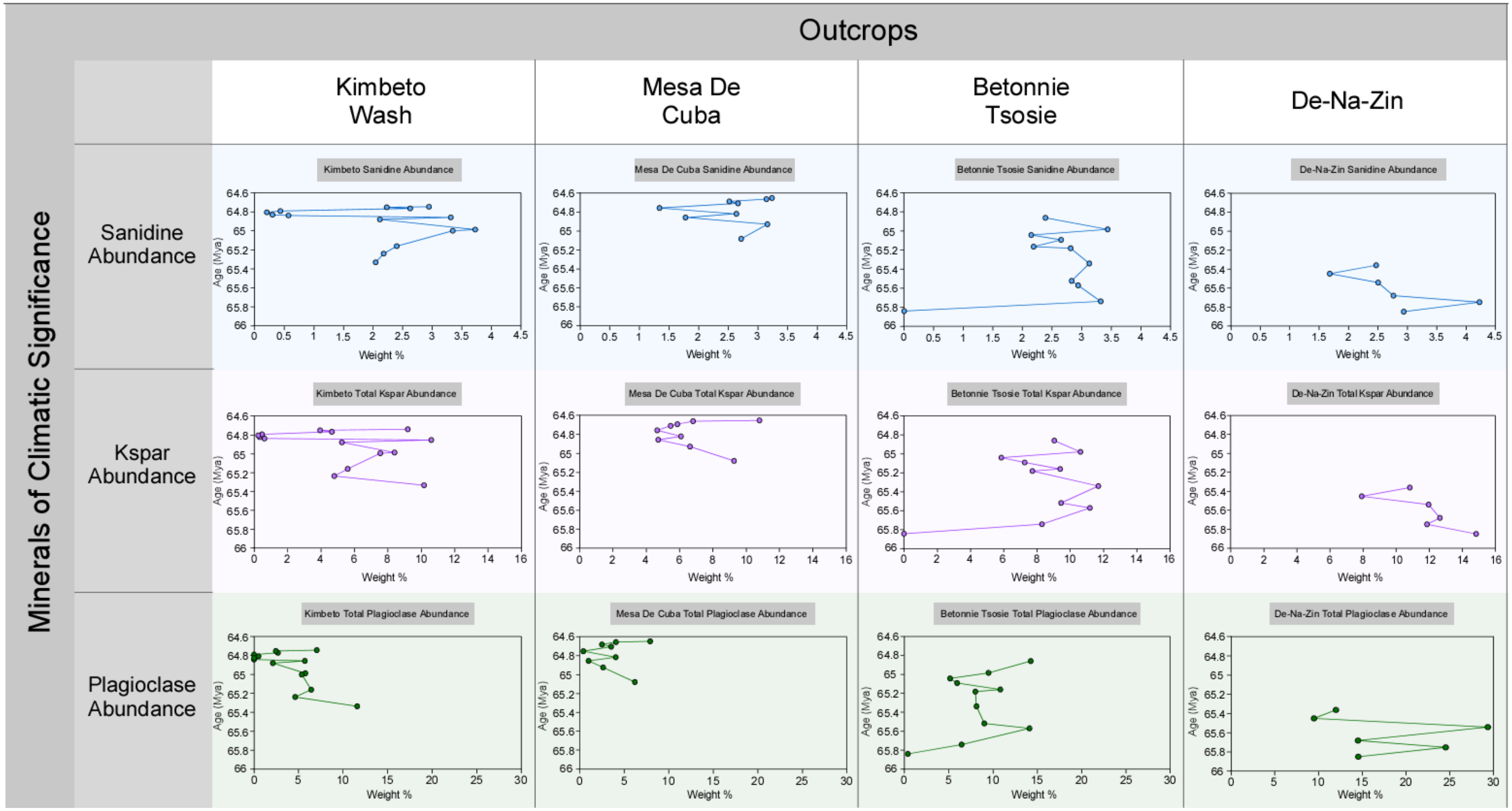

Figure 4.3. Stratigraphic occurrence and abundance of detrital minerals that are sensitive to climate and are likely involved in weathering.

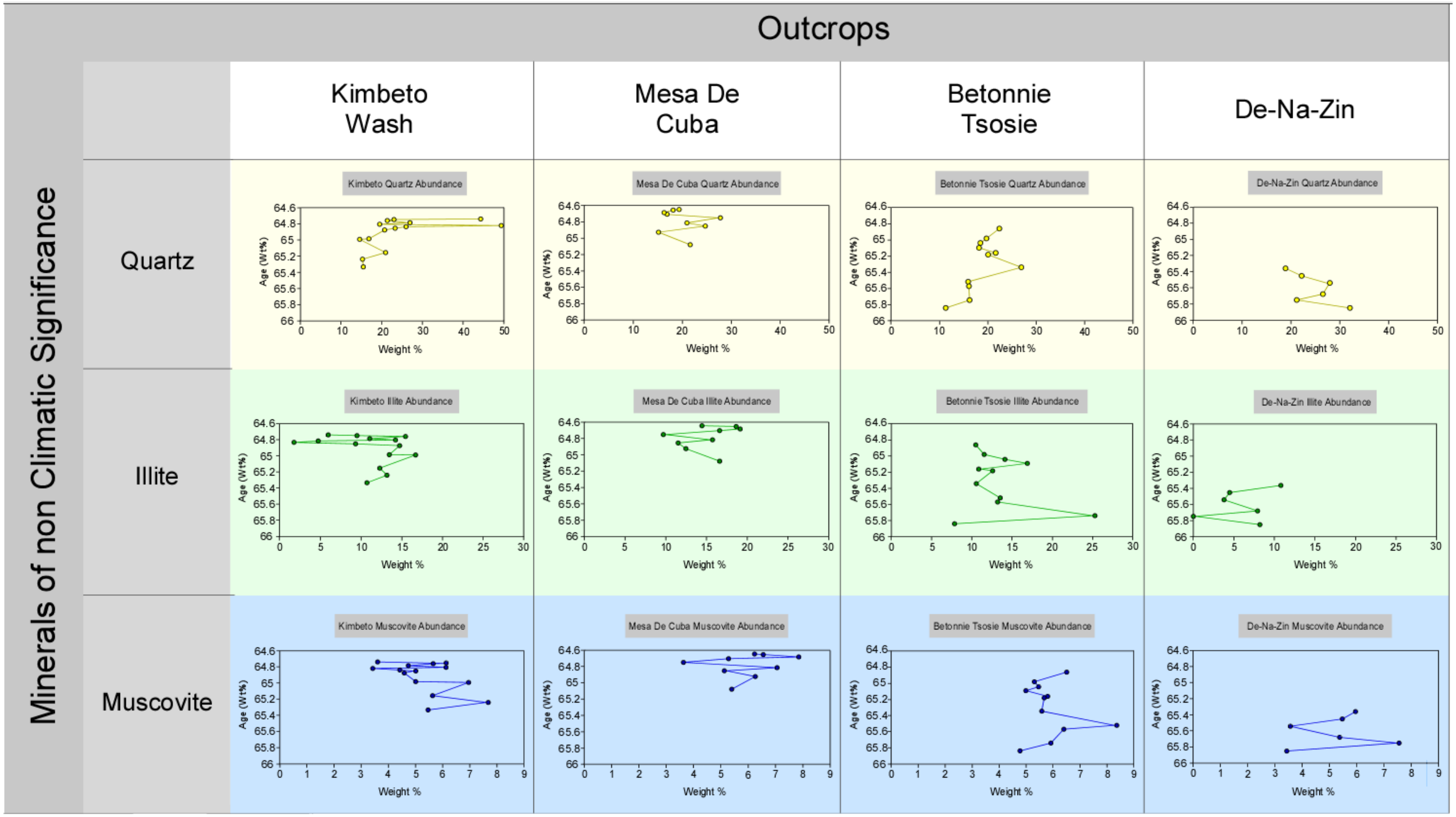

Figure 4.4. Stratigraphic occurrence and abundance of detrital minerals that are resistant to weathering.

Table 4.1. Paleosol mineral abundances for the Kimbeto outcrop.

Sample	Depth (m)	AGE Ma	Sanidine	Total Kspar	Total Plag	Total Fe oxides	Total Kaol.	Total Smectite	Quartz	Illite	Muscovite
P1.1	10.3	65.33	2	10.2	11.6	4	0.5	39.5	15.4	10.7	5.5
P6.1	13.75	65.24	2.2	4.8	4.6	0	2.3	50	15.2	13.2	7.7
P8.1	16.7	65.16	2.4	5.6	6.4	0.7	3.2	43.7	21	12.3	5.6
P9.1	22.65	64.99	3.3	7.5	5.4	1.2	3.9	42	14.6	16.7	6.9
P10.1	22.95	64.98	3.7	8.4	5.7	0.5	2.5	46.5	16.8	13.5	5
P15.1	26.9	64.87	2.1	5.2	2.1	0.9	8.6	42.4	20.7	14.7	4.6
P19.1	28.7	64.85	3.3	10.6	5.7	0	15.8	28.7	23.3	9.3	5
P21.1	31.25	64.83	0.6	0.6	0	0	10	56.5	26	1.8	4.4
P22.1_5	33.15	64.82	0.3	0.3	0	2.1	6.3	33.2	49.3	4.7	3.4
P23.1_5	35.25	64.8	0.2	0.2	0.5	0.5	13.4	44.3	19.5	14.2	6.1
P24.1	37.35	64.79	0.4	0.4	0	0.2	11.6	44.1	27	11.1	4.7
P27.1	41.25	64.76	2.6	4.7	2.7	0	4.4	45	21.4	15.5	5.7
P28.1	42.45	64.75	2.2	3.9	2.5	0	6.1	47.9	23	9.5	6.1
P29.1	43.8	64.74	2.9	9.2	7.1	0.1	9.1	19.8	44.3	6	3.6
		Average:	2	5.1	3.9	0.7	7	41.7	24.1	10.9	5.3

Table 4.2. Paleosol mineral abundances for the Mesa De Cuba outcrop.

Sample	Depth (m)	AGE Ma	Sanidine	Total Kspar	Total Plag	Total Fe oxides	Total Kaol.	Total Smectite	Quartz	Illite	Muscovite
P3.3	14.3	65.08	2.7	9.3	6.2	0.2	2.7	35.4	21.6	16.6	5.4
P4.3	19.9	64.92	3.2	6.6	2.6	0	7.8	45.9	15.1	12.5	6.2
P6.3	23.3	64.85	1.8	4.7	1	0	12.1	40.5	24.7	11.5	5.1
P9.3	27.9	64.82	2.6	6.1	4	0	3.4	40.8	20.9	15.8	7.1
P11.3	35.9	64.75	1.3	4.6	0.4	0.2	13	40.4	27.8	9.7	3.6
P15.3	41.8	64.7	2.7	5.5	3.5	0.1	5.7	44.2	16.9	16.6	5.3
P17.3	44.1	64.69	2.5	5.9	2.5	0	5.6	40.5	16.3	19.2	7.8
P20.3	47.8	64.66	3.1	6.8	4	0.1	3.1	39.7	18.2	18.7	6.5
P21.3	48.95	64.65	3.2	10.8	7.9	0.5	4.5	32.2	19.3	14.4	6.2
		Average:	2.6	6.7	3.6	0.1	6.4	40	20.1	15	5.9

Table 4.3. Paleosol mineral abundances for the Betonnie Tsosie outcrop.

Sample	Depth (m)	AGE Ma	Sanidine	Total Kspar	Total Plag	Total Fe oxides	Total Kaol.	Total Smectite	Quartz	Illite	Muscovite
P1	0.9	65.84	0	0	0.4	5.2	4.8	64.8	11.3	7.8	4.8
P4	4.5	65.74	3.3	8.3	6.5	0.2	4.6	32.5	16.2	25.3	5.9
P9	10.65	65.57	3	11.2	14.1	0.1	1	35.8	16.1	13.2	6.4
P12	12.45	65.52	2.8	9.5	9	0	2.2	38.6	15.9	13.5	8.3
P14	19.1	65.34	3.1	11.7	8.2	0	1.4	35.1	26.9	10.6	5.6
P17	24.85	65.18	2.8	7.7	8	0	2.3	42.8	20.1	12.6	5.7
P19	25.75	65.16	2.2	9.4	10.8	0.7	1.5	37.9	21.6	10.9	5.8
P21	28.1	65.09	2.7	7.3	6	0.3	2.7	42.8	18.2	16.9	5
P24	29.8	65.04	2.1	5.9	5.2	0	5	45.2	18.5	14.1	5.5
P27	32	64.98	3.4	10.6	9.5	0	12.3	29.5	19.6	11.5	5.3
P29	36.65	64.86	2.4	9.1	14.2	0.2	1.4	34.6	22.4	10.5	5.9
		Average:	2.5	8.2	8.4	0.6	3.5	40	18.8	13.4	5.9

Table 4.4. Paleosol mineral abundances for the De-Na-Zin outcrop.

Sample	Depth (m)	AGE Ma	Sanidine	Total Kspar	Total Plag	Total Fe oxides	Total Kaol.	Total Smectite	Quartz	Illite	Muscovite
A	2.45	65.85	2.9	14.8	14.5	0.1	8.3	17.6	32	8.2	3.4
C	6.25	65.75	4.2	11.9	24.5	2.1	6.1	23.6	21.2	0	7.6
D	8.9	65.68	2.8	12.6	14.5	0	5.1	27.1	26.6	7.9	5.4
E	14.2	65.54	2.5	11.9	29.4	0.6	0.6	21.6	28	3.8	3.6
F	17.5	65.45	1.7	7.9	9.4	0.2	4.4	44.6	22.3	4.5	5.5
C 11_2	20.9	65.36	2.5	10.8	12	1.6	1.5	36.1	18.8	10.8	6
		Average:	2.8	11.7	17.4	0.8	4.3	28.4	24.8	5.9	5.2

Mineralogic Comparison Between The Four Outcrops

Because the Betonnie Tsosie outcrop comprises the longest duration of the four outcrops, it is used as a reference of comparison to the other Naciemento outcrops. All the outcrops display similar ranges of mineral abundances with the exception of the De Na Zin section. This section contains only the bottom half of the studied interval and is distinctive because the paleosols have a high abundance of plagioclase and potassium feldspar, as well as a relatively low abundance of smectite.

Stratigraphic Trends Observed In Paleosol Mineral Assemblages

Feldspar and kaolinite abundance exhibit an inverse relationship up section starting at about 65 Ma (Figures 4.2 and 4.3). This stratigraphic trend is particularly well developed in the Kimbeto Wash section where potassium feldspar and plagioclase decline in abundance to less than 1 Wt% while kaolinite increases to greater than 14 Wt%. This trend is also present, although more subtlety, in the Mesa De Cuba and Betonnie Tsosie sections. By 64.7 Ma, kaolinite and feldspar abundances return to pre 65 Ma abundances. This trend cannot be observed in the De Na Zin section because the sedimentary record stops at 65.2 Ma.

Sanidine, Kspar, and plagioclase trends rise and fall in unison throughout all of the outcrops (Figure 4.3). This makes sense since these minerals are easily weathered, so if one decreases in value due to weathering, then it can be expected that the others will follow a similar trend. On the other hand, the trends of kaolinite seem to mirror these minerals throughout all the outcrops, such that while the feldspars decreases in abundance, kaolinite increases in abundance (Figures 4.2 and 4.3).

This trend is particularly evident in Kimbeto Wash when kaolinite at 64.80 Ma has an abundance of 13.42 Wt% while sanidine, kspar, and plagioclase abundances at that age have fallen to 0.207, 0.207, and 0.515 Wt% respectively (Table 4.1).

Within the Mesa De Cuba, kaolinite values increase to 12.07 and 13.01 Wt% at 64.85 and 64.75 Ma respectively. At these same points, sanidine, kspar, and plagioclase values have all fallen below their average, thus their trends are inverse to the kaolinite trends over the same interval (Table 4.2).

In the Betonnie Tsosie at 65.84 and 65.04 Ma, all feldspar values are measured to be below average, while kaolinite values are listed above average (Table 4.3). This trend is reflected in the values where the feldspars decrease, while kaolinite increase (Figures 4.2 and 4.3).

Lastly, this trend is also seen within the De-Na-Zin at sample F (Table 4.4). There, all of the feldspars are below average in value, while kaolinite is recorded to be above average (Figures 4.2 and 4.3).

Another trend to note is the high abundance of kaolinite near the top of the Kimbeto and Mesa De Cuba sections at 64.85, 64.80, and at 64.74 Ma in the Kimbeto section and at 64.85 and 64.75 Ma in the Mesa de Cuba section. Within the Betonnie

Tsosie and the De-Na-Zin, kaolinite values rise again near the base of the section, after a brief period of recorded values being below average at 65.74 and 65.84 Ma in the Betonnie Tsosie and at 65.85 and 65.75 Ma in the De-Na-Zin (Figure 4.2).

CHAPTER FIVE

Discussion

Through the analysis of paleosol mineral assemblages, environmental conditions can be determined based upon the minerals present (Figure 5.1). In the paleosol mineral assemblages, quartz, illite and muscovite are resistant to chemical weathering and are most likely inherited. In contrast, kaolinite, smectite, and hematite are commonly neoformed *in situ*, and thus reflect the climatic conditions in which the paleosol formed. These minerals have different climate thresholds that can be used to qualitatively reconstruct precipitation. Specifically, kaolinite is stable within wetter climates, which facilitates and preserves its formation, so the presence of kaolinite has a significant impact on climate interpretation. Feldspars weather away and turn into clays as conditions get hotter and wetter, but K-spar is more resistant to weathering than plagioclase. Lastly, calcite indicates dry conditions; however, minimal calcite was detected within the samples, suggesting most of the paleosols were formed under conditions of precipitation greater than 800 mm, which is typically the threshold under which pedogenic carbonate forms (e.g., Retallack, 2001). Interpretation of the results of this study are based on the paleo pedogenic threshold concept while taking into account the abundancies of certain climatically informative minerals (Figure 5.1).

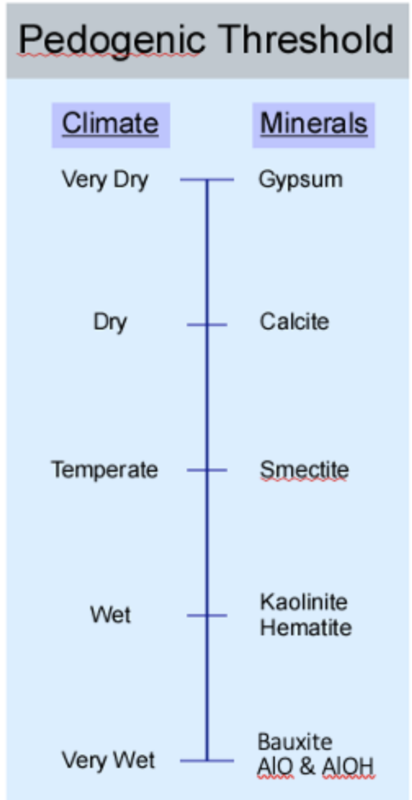

Figure 5.1. A chart depicting the pedogenic threshold concept where various climate conditions is listed on the left and the corresponding minerals that form in those environments is listed on the right.

The stratigraphic distribution of the paleosol mineral assemblages indicates evolving environmental conditions during the early Paleogene (Figure 5.1). Additionally, the presence or absence of particular minerals provides a general climate setting during Naciemento deposition. For example, the lack of pedogenic calcite indicates that mean annual precipitation (MAP) was always greater than 800 mm of rain per year and the presence of kaolinite in all paleosols suggests that MAP was between 1000 to 2000 mm of rain per year (Retallack, 2001).

It appears that conditions became more humid at about 65 Ma based on increasing kaolinite abundance and decreasing feldspar abundance. This short-lived increase in

MAP is documented in three of the four sections in this study. Drier conditions ensued by 64.7 Ma, so the wet interval encompasses about 300,000 years.

The De-Na-Zin section has more feldspar and a lower abundance of kaolinite and smectite than the other sections (Figures 4.2-4.4). This could mean that the De-Na-Zin section may record drier conditions when weathering intensity was low and feldspars were not reacting and turning into clay minerals. However, given that the De-Na-Zin section is time equivalent to the other section, this is unlikely. Alternatively, the higher abundance of feldspar at De-Na-Zin probably indicates that it experienced less weathering than the other three sections. This could be due to a landscape position that resulted in poorer drained soils. Poor drainage inhibits weathering by preventing the solutes from being removed from soil pore waters.

The abundance of smectite does not exhibit stratigraphic trends, even though it is probably the most common weathering product in soils. The lack of stratigraphic trends for smectite may be due to the large amount of inherited smectite that may mask the formation of pedogenic smectite during weathering.

CHAPTER SIX

Conclusion

Quantitative X-ray diffraction performed on early Paleogene paleosols in the San Juan Basin reveals that the paleosol mineral assemblages are composed of smectite, quartz, illite, plagioclase, potassium feldspar, kaolinite, muscovite, and hematite (listed in order of decreasing abundance). The abundance of the minerals illite, quartz, muscovite, and smectite do not exhibit stratigraphic trends and are interpreted as being primarily inherited when the overbank muds were deposited. These minerals are apparently not sensitive to climatic conditions during pedogenesis. In contrast, the inherited feldspar minerals display distinct stratigraphic trends. The abundance of the feldspar was altered during pedogenesis and thus can be used to reconstruct climate-controlled weathering intensity. The abundance of kaolinite also displays stratigraphic trends and is interpreted as a neoformed soil mineral that reflects environmental conditions.

Based upon the X-ray diffraction results a paleoclimate reconstruction can be made for the time period observed (Figure 6.1).

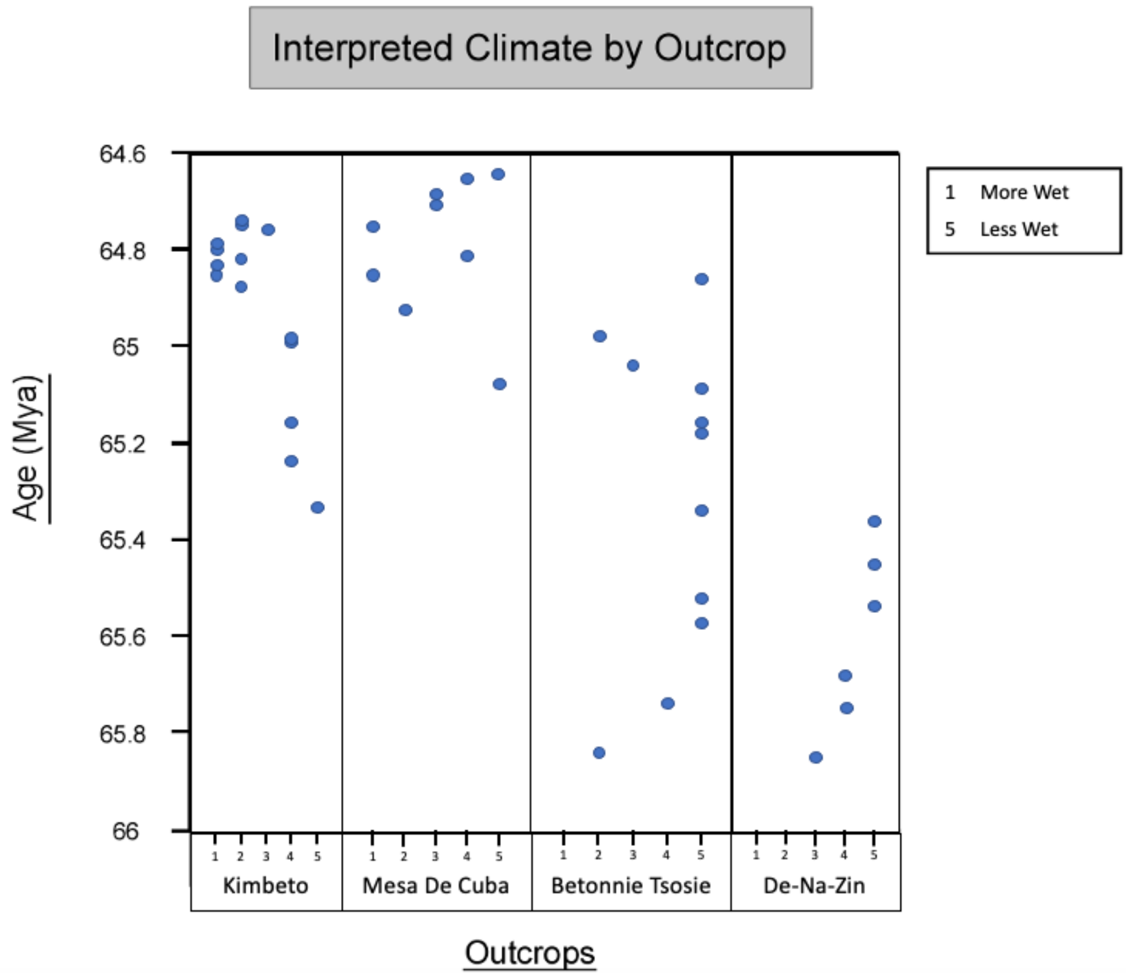

Figure 6.1. A paleoclimate reconstruction made from all the samples analyzed from each outcrop organized by age with the interpreted climate represented at each point. In this case, a drier climate indicates a climate that is less wet than previous observations and has a MAP above 1000 mm due to the presence of kaolinite.

Overall, the climate in the San Juan Basin during the early Paleogene was fairly wet as indicated by the presence of kaolinite throughout all of the sections. There were no dry periods indicated in any of the sections since the abundance of calcite had been undetectable. However, some parts of the section were wetter than others based upon the varying abundance of kaolinite and the feldspars. Feldspar abundance is indicative of weathering conditions that create kaolinite and this negative correlation in mineral abundances is recognized in the upper part of the studied section indication increasing amounts of precipitation. Therefore, after the K/Pg boundary the climate was wet during the deposition of the basal Nacimiento Formation and conditions became progressively wetter near the top of the section (Figure 6.1).

WORKS CITED

Cather, S. M., Heizler, M. T., & Williamson, T. E. (2019). Laramide fluvial evolution of the San Juan Basin, New Mexico and Colorado: Paleocurrent and detrital-sanidine age constraints from the Paleocene Nacimiento and Animas formations. *Geosphere*, *15*(5), (pp. 1641-1664).

Cather, S. M., Mack, G. H., & Giles, K. A. (2004). Laramide orogeny in central and northern New Mexico and southern Colorado. *The Geology of New Mexico, A Geologic History: New Mexico Geological Society Special Publication*, *11*, (pp. 203-248).

Chadwick, O. A., & Chorover, J. (2001). The chemistry of pedogenic thresholds. *Geoderma*, *100*(3-4), (pp. 321-353).

Davis, A. J., Peppe, D. J., Atchley, S. C., Williamson, T. E., & Flynn, A. G. (2019). Climate and landscape reconstruction of the Arroyo Chijuillita Member of the Nacimiento Formation, San Juan Basin, New Mexico: Providing environmental context to early Paleocene mammal evolution. Baylor University Master's Thesis.

Ebrel, DD. (2003), User’s guide to ROCKJOCK – A program for determining quantitative mineralogy from powder X-ray diffraction data, USGS Open-File Report 03-78, 48 p.

Fassett, J. E. (1974). Cretaceous and tertiary rocks of the eastern San Juan Basin, New Mexico and Colorado. In *New Mexico Geological Society Guidebook, 25th Field Conference, Ghost Ranch, Central-Northern New Mexico* (pp. 225-230).

Fassett, J. E., & Hinds, J. S. (1971). *Geology and fuel resources of the Fruitland Formation and Kirtland Shale of the San Juan basin, New Mexico and Colorado*. US Government Printing Office. (pp. 4-6, 28).

Flynn, A. G., Davis, A. J., Williamson, T. E., Heizler, M., Fenley IV, C. W., Leslie, C. E., ... & Peppe, D. J. (2020). Early Paleocene Magnetostratigraphy and Revised Biostratigraphy of the Ojo Alamo Sandstone and Lower Nacimiento Formation, San Juan Basin, New Mexico, USA. *Geological Society of America Bulletin*.

Lindsay, E. H., Jacobs, L. L., & Butler, R. F. (1978). Biostratigraphy and magnetostratigraphy of Paleocene terrestrial deposits, San Juan Basin, New Mexico. *Geology*, *6*(7), (pp. 425-429).

Ogg, J. G. (2020). Geomagnetic polarity time scale. In *Geologic time scale 2020* (pp. 159-192). Elsevier.

Powell, J. S. (1973). Paleontology and sedimentation models of the Kimbeto Member of the Ojo Alamo Sandstone. *Four Corners Geological Society Memoir Book* (pp.111-122).

Retallack, G.J., 2001, Soils of the past, Blackwell Science Ltd., Second Edition, p. 117

Williamson, T. E., Nichols, D. J., & Weil, A. (2008). Paleocene palynomorph assemblages from the Nacimiento Formation, San Juan Basin, New Mexico, and their biostratigraphic significance. *New Mexico Geology*, *30*(1), (pp. 3-11).